Bioconjugate Chemistry

Article

pubs.acs.org/bc

Quantum Dot Lipid Oligonucleotide Bioconjugates: Toward a New Anti-MicroRNA Nanoplatform

Ahissan Aimé, Nataliia Beztsinna, Amit Patwa, Alexander Pokolenko, Isabelle Bestel,* and Philippe Barthélémy*

Universite Bordeaux, ARNA laboratory, F-33000 Bordeaux, France, and INSERM, U869, ARNA laboratory, F-33000 Bordeaux, France

Supporting Information

ABSTRACT: The construction of new nanotools is presented here using the example of fluorescent semiconductor nanocrystals, quantum dots (QDs). In this study, the implementation of the new lipid oligonucleotide conjugate-functionalized quantum dots (LON-QDs) is realized in four steps: (i) the synthesis of the lipid oligonucleotide conjugates (LONs), (ii) the encapsulation of QDs by nucleolipids and LONs, (iii) the study of the duplex formation of LON-QDs with the complementary ON partners, and (iv) the cellular uptake of the LON-QD platform and hybridization with the target ONs (microRNA and miR-21).

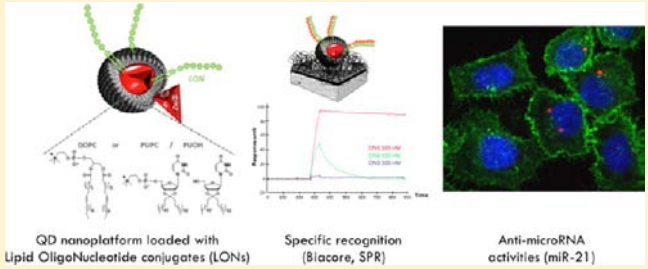

INTRODUCTION

A fundamental objective in biology is to elucidate the role and the fate of biomolecules in living cells, which still requires new approaches, technologies, and tools. To address these bioimaging issues, nanocrystalline semiconductors, namely quantum dots (QDs), are promising nanosystems.[1−3] QDs, which are inorganic (CdSe, CdS, CdTe, etc.) nanomaterial (2−6 nm), possess remarkable optical, electronic, magnetic, and even chemical features.[4,5] Their properties have been investigated in various scientific domains, including biology[6−8] and biomedicine,[9] computing and memory,[10] electronics,[11] optoelectronic devices,[12] lighting and lasers,[13] and sensor applications.[14]

Despite the numerous functionalization strategies investigated so far, the surface coating of QDs with biomolecules remains a challenge in many cases.[15] Functionalized QDs have been widely constructed via ligand exchange with thiol- or histidine-bearing molecules and covalent linkages involving surrounding QD ligands (lipids[16] and copolymers).[17] Considering the functionalization of QDs with oligonucleotides, different approaches have been reported, including covalent coupling,[18,19] high-affinity ligand−receptor recognition (biotin/streptavidin),[18,20−22] and noncovalent interactions using mainly electrostatic adsorption.[23,24] Among the main drawbacks observed for the QDs functionalized via electrostatic interactions, one can mention the instability of the systems caused by the variation of pH and/or ionic strength, the relative weakness of the adsorption, and the limited number of copies of adsorbed oligonucleotides per QD.[23] Less common, although highly promising, the insertion of modified oligonucleotide via hydrophobic anchoring in a QD nanoplatform encapsulated with lipids could overcome these drawbacks.

Here we demonstrate that lipid oligonucleotide conjugates (LONs)[25] targeting microRNAs can be used to functionalize QDs. We show that the combination of the solubilization−functionalization strategy with optimized amphiphilic oligonucleotide functionalities and lipids is an efficient approach for providing oligonucleotide-based QDs with recognition and detection properties.

RESULTS AND DISCUSSION

New nanoplatforms based on QDs hold great promise for the development of biological labeling applications, intracellular sensors, deep-tissue and tumor imaging agents, and sensitizers for photodynamic therapy or drug delivery by virtue of their unique optical properties.[1] Nevertheless, biological exploitation of QDs involves several steps of functionalization. Because of the fluorescent behavior of QDs,[4,5] several strategies mainly based on covalent linkers[18,19] or electrostatic adsorption[23,24] were developed. The first one requires surface chemistry that is not trivial; the second is highly dependent on pH, and a low rate of functionalization is encountered.[23,24] In this context, the anchoring of LON at the QD hydrophobic surface, a strategy very promising for functionalization in terms of robustness and ease of handling, has never been investigated. The implementation of our ON-based nanoplatform was realized by a procedure achieved in three steps. First, LONs were synthesized via two different approaches: 1,3-dipolar cycloaddition click and phosphoramidite reactions. In a second step, QDs possessing a native hydrophobic shell [trioctylphosphine

Received: March 28, 2013
Revised: July 2, 2013
Published: July 26, 2013

dx.doi.org/10.1021/bc400157z | Bioconjugate Chem. 2013, 24, 1345−1355

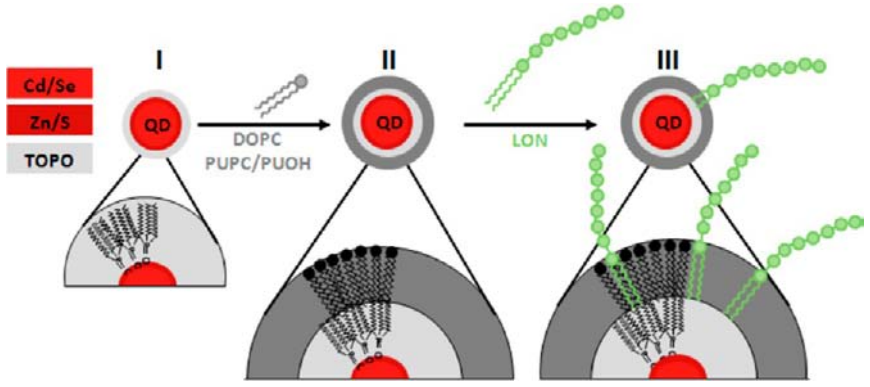

Figure 1. Schematic drawing illustrating the different steps leading to the implementation of the nanoplatform. In parallel with the synthesis of LONs (green), hydrophobic QDs were encapsulated by amphiphiles (DOPC, PUPC, and PUOH). In a final step, the QD-LON nanoplatform was isolated after insertion of LONs into the amphiphile layer.

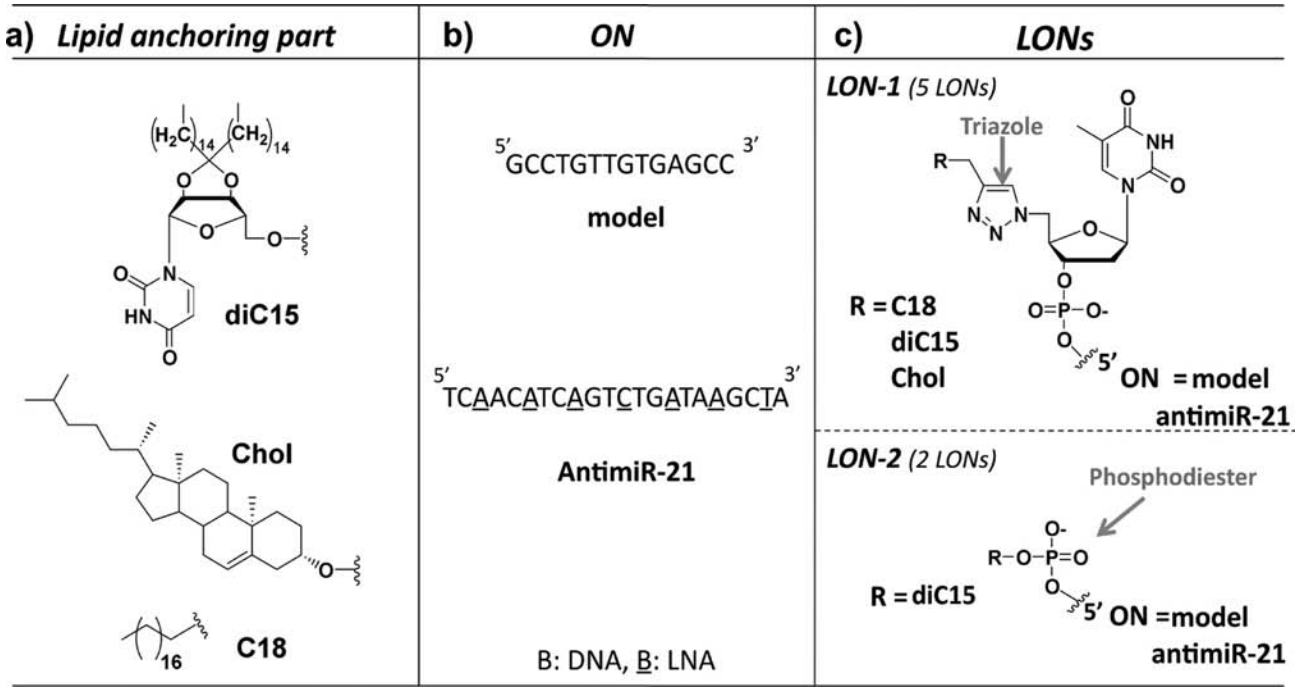

Figure 2. Chemical structures of LONs. (a) Three different lipid parts used in this work, including diC15, cholesterol, and C18. (b) Two oligonucleotide sequences: full DNA 14-mer (model) and 22-mer (antimiR-21) featuring LNA nucleotide (A, T or C). (c) 1,2,3-Triazole and phosphodiester linkers.

oxide (TOPO)] were encapsulated and solubilized in water by a layer of amphiphiles. This water solubilization approach offers two advantages: (i) it preserves the optical properties of the QD, and (ii) it leads to the formation of a micelle that represents an ideal support for LON anchoring at the QD surface. Finally, in a third step, LONs were inserted at the QD surface via the anchoring of their hydrophobic moieties into the amphiphile layer (Figure 1).

Synthesis of LONs. The structural and functional robustness of the proposed soft hybrid ON/QD nanoplatform relies on the design of LON and initial selection of membrane anchoring. The insertion of LON into membranes is not a trivial issue because these amphiphiles tend also to self-aggregate in aqueous solutions in the absence of a membrane. LONs featuring one lipid anchor could be poorly inserted into membranes, whereas LONs with two lipid anchors may tend to form stable supramolecular structures in aqueous solution, making their insertion into membranes difficult.[26−28] Herein, three different lipid anchors were selected, including a cholesteryl, a satured C18 alkyl chain, and a di-C15 ketal motif (Figure 2a) that has previously caused membrane anchoring on DNA-tagged liposomes made of DOPC.[29]

With regard to the ON part, two sequences were studied (Figure 2b): (i) the first (named model) being a DNA model selected to avoid self-complementary strands and yield a melting temperature (T_m) of 37 °C for a 14-mer DNA duplex and (ii) the second (named antimiR) being a biologically relevant 23-mer LNA/DNA sequence antisense oligonucleotide directed against the microRNA miR-21, a microRNA strongly overexpressed in many cancers and associated with pessimist prognostics.[30] The synthesis of these ONs was straightforward using classical phosphoramidite chemistry. From these lipids and ON parts, different LONs were engineered depending on the conjugation step (Figure 2c). Two main strategies were

dx.doi.org/10.1021/bc400157z | Bioconjugate Chem. 2013, 24, 1345−1355

Scheme 1. Synthetic Pathways Leading to a LON (compound 6)[a]

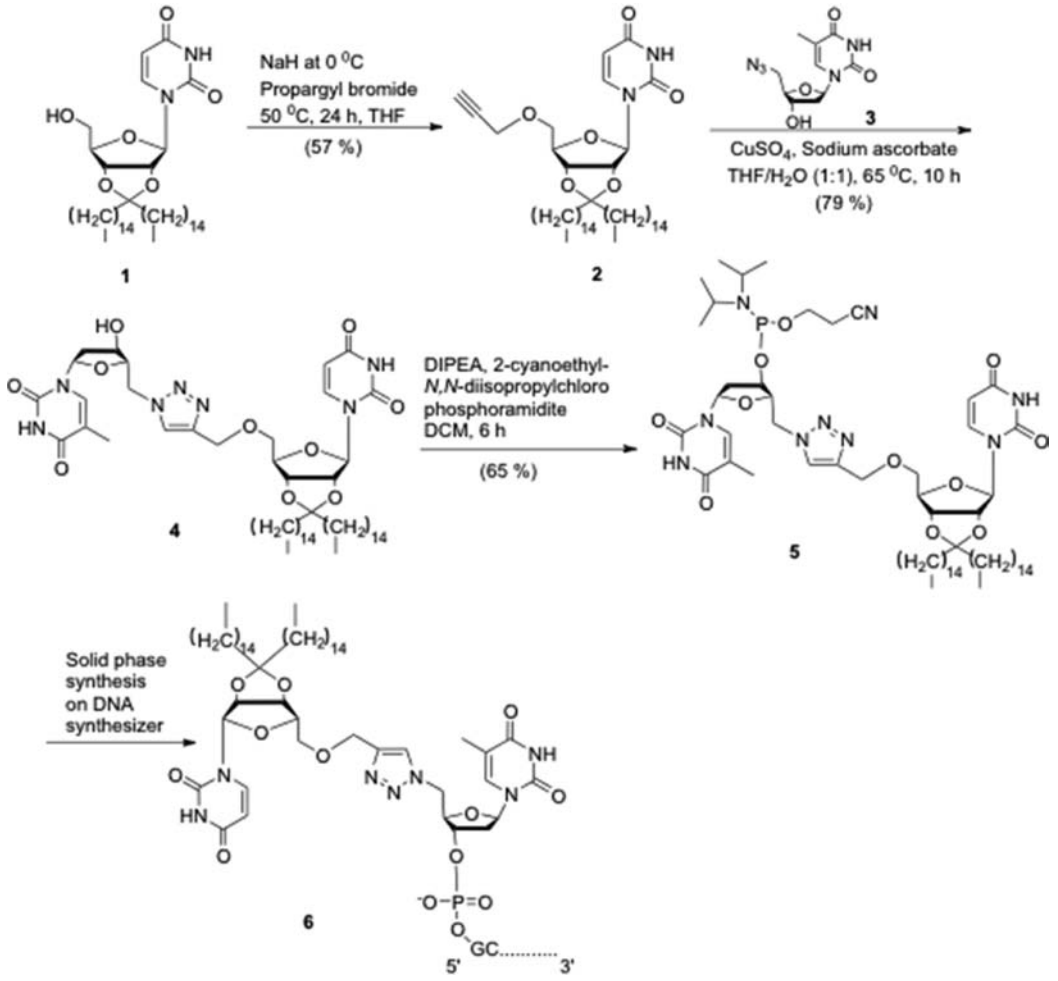

[a]After the synthesis of the customized phosphoramidites (**5**), which is realized in three steps starting from ketal nucleoside **1**, compound **5** is reacted with the 5′-extremity during the oligonucleotide synthesis (3′-to-5′ elongation).

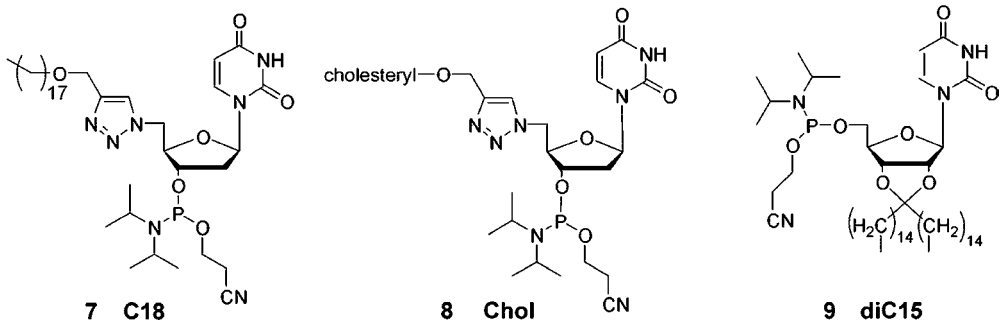

Figure 3. Previously described phosphoramidites **7**, **8**,[31] and **9**.[29]

investigated: the first exploiting a cycloaddition click reaction and leading to a triazole linker[31] (LON-1 family) and the second relying on a previously described head-to-head (5′-to-5′) phosphodiester linker (LON-2 family).[29] Both strategies lead to a compact QD nanoplatform that could evolve to molecular beacon systems. Because of the lack of a spacer between the ON part and the lipid moiety of LON, the ON part will be in close contact with the multiple headgroups of amphiphiles at the QD surface triggering potential noncovalent interactions. In this context, a variation in the linker conjugation chemistry could hardly impact the hybridization step.

In the first strategy, a 5′-azido desoxyribo thymidine **3** was synthesized as previously reported and coupled through a 1,3-dipolar cycloaddition mediated by Cu(I) to C18, cholesteryl, and the diC15 motif possessing a terminal alkyne group. The former have previously been described,[31] and the latter was synthesized from ketal uridine **1** after propargylation of the 5′-hydroxyl group (compound **2**) (Scheme 1). Phosphoramidite **5** was then generated, and the different phosphoramidite synthetic blocks **5**, **7**, and **8** (Figure 3) consisting of a

dx.doi.org/10.1021/bc400157z | Bioconjugate Chem. 2013, 24, 1345−1355

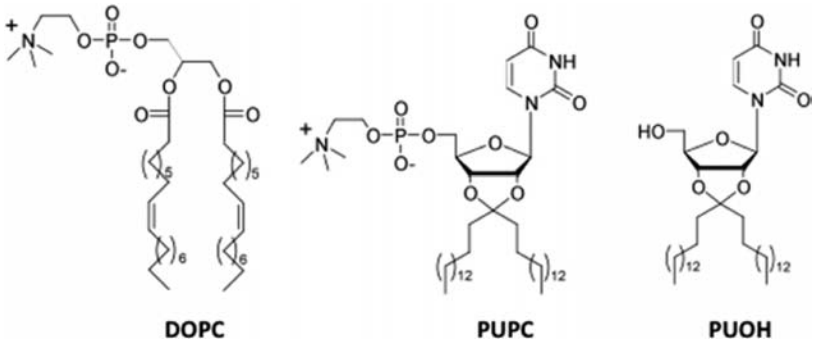

Figure 4. Amphiphiles used for QD water solubilization, including a lipid (DOPC) and two nucleolipids (PUPC and PUOH).

thymidine conjugated by click reaction to the different lipid parts were incorporated in the 5′-extremity of each ON (model and antimiR). The second strategy, used for only the diC15 motif, relies on the synthesis of a 5′-phosphoramidite derived from ketal uridine **9** described previously (Figure 3).[29]

Finally, five LONs based on the first strategy (C18-model-1, chol-model-1, C18-antimiR-1, chol-antimiR-1, and diC15-antimiR-1) and two LONs based on the second strategy (diC15-model-2 and diC15-antimiR-2) were synthesized (Figure 2), purified by reverse phase high-performance liquid chromatography (HPLC), and checked by mass spectrometry.

LON-QD Nanoplatform Implementation. The encapsulation of QDs in amphiphiles was investigated to render them water-soluble. For that purpose, natural phospholipids (DOPC) were used as well as synthetic phospholipids such as nucleolipids (PUPC and PUOH),[32] the latter leading to a more compact bilayer compared to the former (Figure 4).[33,34] Selected QDs had a core−shell structure of CdSe/ZnS. These QDs were roughly 6.5 nm in hydrodynamic diameter, with a fluorescence emission peak at 620 nm and a nearly 80% quantum yield.

The water solubilization step relied on the encapsulation of QD in a phospholipid micelle according to the protocol of Dubertret.[35] A homogeneous mixture of QDs in toluene and phospholipids (DOPC or PUPC and PUOH) in chloroform was prepared, and then a film was obtained after solvent evaporation. A suspension of QD micelles was generated after water had been added to the film. Several purification steps were then performed to remove empty micelles and micelle aggregates. It should be noted that the stoichiometry between QD and phospholipids is a crucial parameter because a ratio of <100 equiv of phospholipid per equivalent of QD led to aggregation and encapsulation of several QDs per micelles. The increase in the concentration of phospholipids significantly reduced the size of micelles. Three types of QD micelles were prepared: DOPC-QD micelles, PUPC-QD micelles, and PUOH/PUPC-QD micelles (according to the fact that PUOH alone was demonstrated to be unable to self-assemble in bilayers).

LON-QD nanoplatforms were formed by mixing QD micelles and LON for at least 1 h at 37 °C prior to use. The amount of DNA grafted to QD was quantified after extensive purification procedures with a membrane filter [10 kDa molecular weight cutoff (MWCO)]. The UV absorption of the filtrate at 260 nm was measured to calculate the amount of ungrafted LON. Following the reaction of QDs with 50, 100, or 250 equiv of LON per equivalent of QD, the fluorescence spectra were measured and 20 LON molecules per QD were found to be grafted in each case (see the Supporting Information). This result is independent of the ON size (14- or 23-mer), which strongly differs from ON-QD platforms based on electrostatic charge interactions. For instance, Lee et al. observed that a maximum of five ON molecules (25-mers) per QD could be bound to a QD possessing a similar diameter after the solubilization step.[23]

LON-QD Nanoplatform Characterization. At the first encapsulation step, several physicochemical characterizations were performed. Dynamic light scattering data, ζ potential analysis, fluorescence spectra, and transmission electron micrographs are reported in Figure 5 for DOPC-QD micelles.

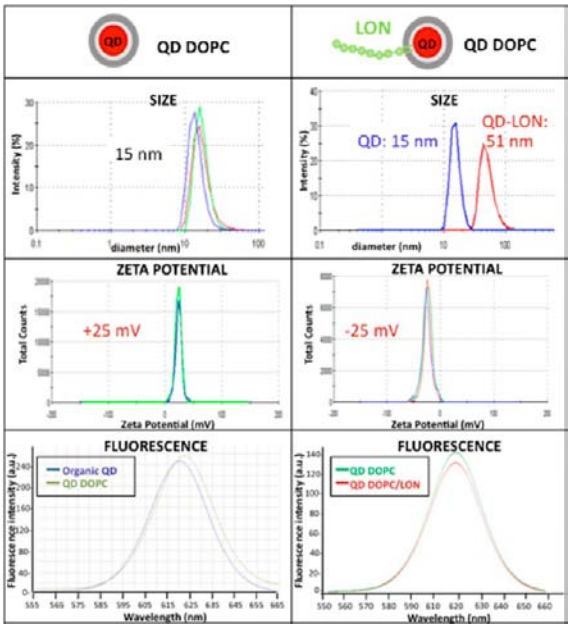

Figure 5. Physicochemical data (size and ζ potential by using DLS and fluorescence) of QD DOPC (left) and LON-DOPC-QD nanoplatforms (diC15-antimiR-1-LON/DOPC-QD) (right).

The QD hydrodynamic diameter increased from 10 to 15 nm in water or in buffer, and micelles had a slight positive charge despite the zwitterionic structure of phospholipids. It is presumably due to the exposition of the ammonium group to the QD surface. The encapsulation did not weaken the fluorescence properties of the central QD with a λ_{max} emission at 620 nm, and transmission electron microscopy, used as a qualitative method for evaluating QD micelle structure, revealed a spherical shape and monoencapsulation. Interestingly, QDs encapsulated by nucleolipids displayed larger diameters (34 nm for PUPC and 65 nm for the 25/75

dx.doi.org/10.1021/bc400157z | Bioconjugate Chem. 2013, 24, 1345−1355

PUPC/PUOH mixture) than DOPC-QD micelles (see the Supporting Information).

Not surprisingly, LON grafting at the QD surface globally increased the QD diameter, which corresponds to 51 nm, and the ζ potential has a negative charge because of the presence of negative phosphodiester functions on LONs. Note that no significant differences in diameters were observed for model versus antimiR LONs. Despite the enhanced QD platform diameter, LON anchoring had no impact on the QD fluorescence properties. Finally, TEM analysis showed the formation of spherical nano-objects that were larger than the corresponding QD before functionalization, which is in agreement with DLS data.

***In Vitro* Hybridization Studies.** The kinetic and equilibrium constants (k_{on}, k_{off}, and K_d) of the LON-QD−ON complexes were assessed by using surface plasmon resonance (SPR) (Biacore). SPR was exploited to follow in real time the interaction of the sensor chip-immobilized LON-QD with the ON target (Figure 6).

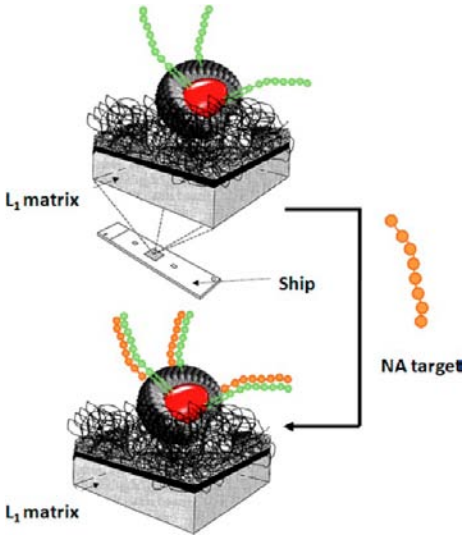

Figure 6. Illustration showing a LON-DOPC-QD nanoplatform trapped onto a matrix embedded in a Biacore ship. This functionalized ship can be used for SPR experiments in the presence of a nucleic acid (NA).

According to previous data on liposomes decorated with LONs,[29] LON-QD nanoplatforms were immobilized onto a hydrophobic dextran surface (i.e., L1 chip from Biacore). To the best of our knowledge, this is the first example of QD immobilization on a SPR sensor chip and of hybridization monitoring at the QD surface based on SPR experiments. The hybridization properties allowed both the evaluation of LON anchoring at the QD surface depending on the hydrophobic behavior of their lipid part and the determination of kinetic parameters of the target recognition at the QD surface to investigate how the presence of LON on the QD can modulate the binding properties of the modified ON. The obtained sensorgrams were fit assuming a one-step reaction, and the kinetic constants for each LON-QD construction determined from direct curve fitting of the sensorgram are listed in Table 1.

The results confirmed the fact that lipidlike hydrophobic parts were essential for a stable anchoring of LON in a bilayer. chol-LON- or C18-LON-grafted liposomes or QD (DOPC-QD or PUPC/PUOH-QD) did not interact with their ON target, certainly reflecting the lack of LONs at the QD surface.

With regard to diC15-LONs, the different sensorgrams revealed no main differences between LON-QD and LON liposomes [neither on the sensor chip immobilization rate (3000 > RU) nor on the specificity of hybridization with complementary ONs]. This was demonstrated for the LON diC15-model-2 grafted on the DOPC-QD platform. As attempted, kinetic analysis of duplex formation with partially (truncated 9-mer sequences) or fully complementary ONs revealed a higher dissociation constant (K_d) for the latter than for the former (Figure 7a). Responses were concentration-dependent and reproducible in both cases (Figure 7b,c), demonstrating the stability of the platform and the fact that the k_{off} values are more related to the hybrid dissociation than the dissociation of LON from the QD. This was further confirmed by the lack of alteration of the amount of LON-QD immobilized during regenerative steps. Moreover, a response was detected preferentially for complementary ONs, while a scrambled sequence that cannot be hybridized was not detected even injected at concentrations of up to 1 μM, demonstrating the specificity of the recognition. Interestingly, LON-QDs induce a slightly lower K_d than the corresponding LON liposomes whatever the size of the ON (model or antimiR) (Table 1). The nature of LON linkers has no significant impact on K_d values, the diC15-antimiR-2 being derived from a phosphodiester linker leading to a quite similar K_d compared to that of diC15-antimiR-1 being derived from a cycloaddition click reaction. Note that for each LON-QD platform evaluation, responses were not observed using nontagged QDs, demonstrating that the observed interactions are due to specific recognition events.

Importantly, using nucleolipids instead of natural phospholipids for QD encapsulation led to an improvement in the K_d for a given oligonucleotide in the case of PUPC. Likely, this

Table 1. Kinetic Constants (k_{on} and k_{off}) and the Resulting Dissociation Constants (K_d) Measured by SPR Analysis on Four Different Systems[a]

	liposomes (DOPC)			QD (DOPC)		
LON sequence	k_{on} ($\times 10^5$ M^{-1} s^{-1})	k_{off} ($\times 10^{-5}$ M^{-1} s^{-1})	K_d (nM)	k_{on} ($\times 10^5$ M^{-1} s^{-1})	k_{off} ($\times 10^{-5}$ M^{-1} s^{-1})	K_d (nM)
diC15-model-2	3.8 ± 0.2	16.3 ± 4.3	0.43 ± 0.1	8.56 ± 0.9	34.1 ± 2	0.38 ± 0.2
diC15-antimiR-2	0.16 ± 0.03	14.2 ± 3.7	8.59 ± 0.8	0.33 ± 0.05	16.1 ± 2.7	5.04 ± 0.71
diC15-antimiR-1	nd	nd	nd	0.33 ± 0.02	9.85 ± 5.9	2.96 ± 1.8
	QD (PUPC)			QD (PUPC/PUOH)		
LON sequence	k_{on} ($\times 10^5$ M^{-1} s^{-1})	k_{off} ($\times 10^{-5}$ M^{-1} s^{-1})	K_d (nM)	k_{on} ($\times 10^5$ M^{-1} s^{-1})	k_{off} ($\times 10^{-5}$ M^{-1} s^{-1})	K_d (nM)
diC15-antimiR-2	0.24 ± 0.02	4.98 ± 0.07	2.11 ± 0.1	0.18 ± 0.04	24 ± 12.7	12.7 ± 4.2

[a]Values are means ± standard deviations of at least three independent experiments.

dx.doi.org/10.1021/bc400157z | *Bioconjugate Chem.* 2013, 24, 1345−1355

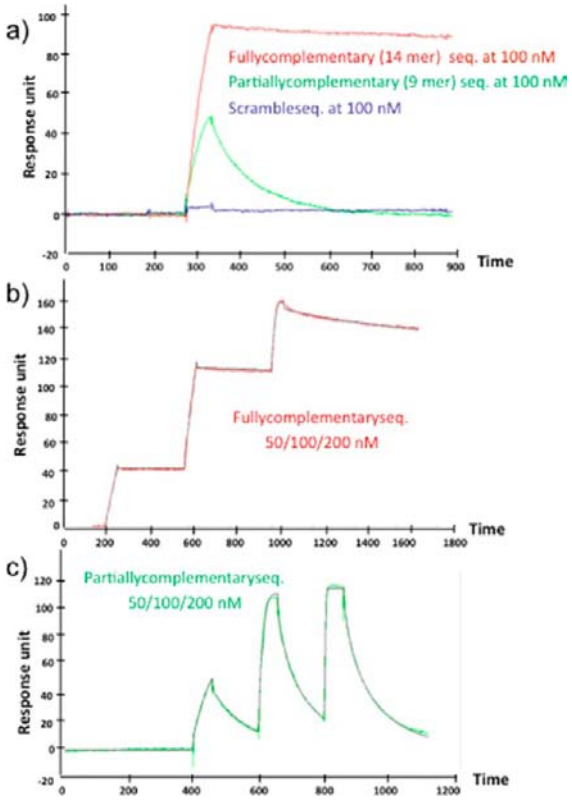

Figure 7. SPR sensorgrams of model-LON-DOPC QD hybridization: red for fully complementary sequence (14-mer), green for partially complementary sequence (9-mer), and blue for scramble sequence (14-mer). (a) Fully and partially complementary sequences (scramble). (b) Dose-dependent response for fully complementary sequence. (c) Dose-dependent response for partially complementary sequence.

result is a consequence of the strongly packing membrane generated by nucleolipids stabilizing the hydrophobic anchoring of LON at the QD surface. The use of a nucleolipid PUPC/PUOH mixture of encapsulation resulted in a decrease in affinity (K_d of 12.7 ± 4.2 nM compared to a K_d of 5.04 ± 0.71 nM for the DOPC formulation) due to the very strong packing of membranes triggered by the PUOH nucleolipid.[33,34] From these observations, we hypothesized that the bilayer packing parameter contributes to the stabilization of the hydrophobic anchoring of LON.

Intracellular Hybridization Studies. According to SPR results, biological evaluations were performed with nanoplatforms composed of diC15-antimiR-1-LON or diC15-antimiR-2-LON grafted on a DOPC-QD surface.

To determine LON-QD cell uptake and further hybridization with target microRNA, HeLa cells were incubated with either nontagged QDs (DOPC-QD) or LON-QDs (diC15-antimiR-1-LON/DOPC-QD) assembled at a QD:LON ratio of 1:20. Figure 8A shows epifluorescence/phase-contrast image overlays of HeLa cells that were incubated with QD platforms at a concentration of 5 nM for 4 h. To visualize the nuclei, the cells were also stained with Hoechst. Punctuate QD fluorescence was dispersed throughout the cytoplasm as well as in the proximity of the cell nuclei. Confocal microscopy experiments with these same samples confirmed that the QD fluorescence was localized exclusively inside the cells with no evidence of QDs entrapped in the cell membranes (Figure 8B). Standard washing of the cells with PBS was sufficient to remove all loosely bound QDs from the cell surface. These experiments demonstrated that LON-QD nanoplatforms are taken up by the cells without using any transfection agents.

Different studies using live cell imaging have established that QDs were internalized by endocytosis.[36,37] A possible drawback of the endocytotic pathway is to avoid the endosomal trapping of QDs to reach the cytoplasm compartment. To test whether LON-QDs were able (i) to penetrate the cytoplasm and (ii) to specifically hybridize with endogenous microRNA-21, quantitative real-time polymerase chain reaction (RT-PCR) experiments were performed after incubation (in the absence of a

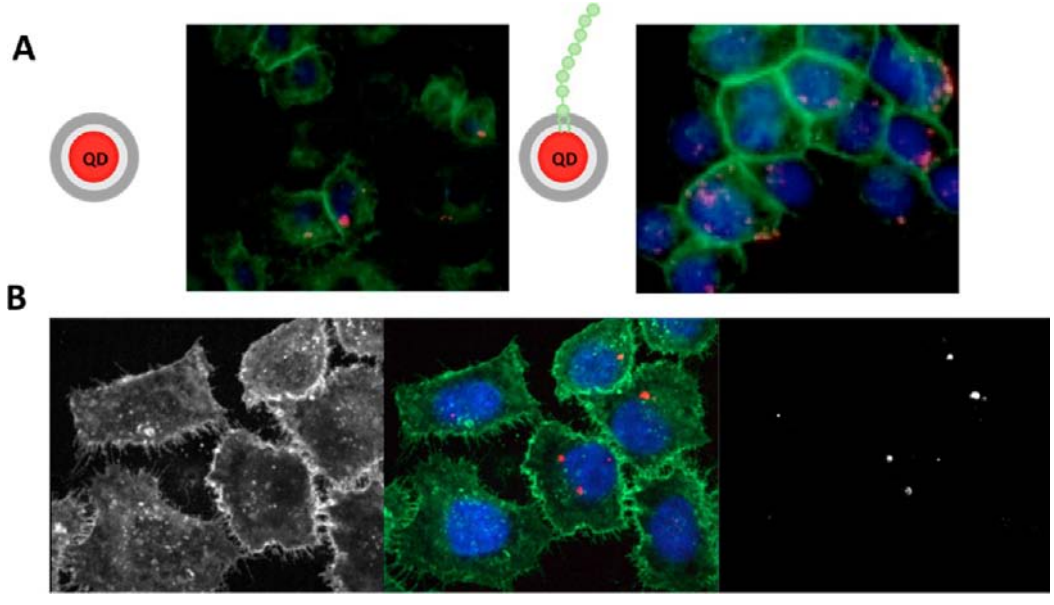

Figure 8. (A) Epifluorescence images of cell uptake of nontagged QDs (left) and antimiR-LON-QDs (right) after incubation in HeLa cells for 4 h. (B) Confocal images of cell uptake of nontagged QDs after incubation in HeLa cells for 4 h. Green for AlexaFluor 488 cell membrane staining, blue for Hoechst 33342 nucleus staining, and red for QD platforms.

dx.doi.org/10.1021/bc400157z | *Bioconjugate Chem.* 2013, 24, 1345−1355

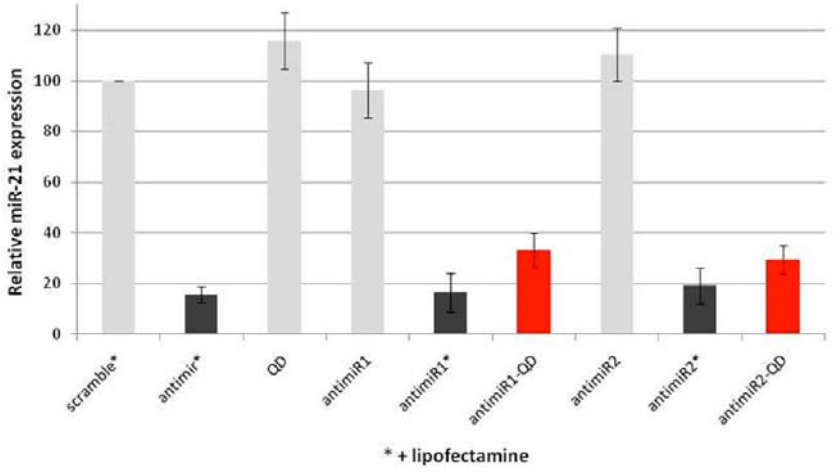

Figure 9. Quantitative RT-PCR experiments. HeLa cells were incubated in the presence of (i) different lipofectamine formulations, including scramble oligonucleotide, antimir, antimiR-1, and antimiR-2, and (ii) QDs, antimiR-1, antimiR-QD, antimiR-2, and antimiR-2-QD. QD nanoplatforms loaded with LONs (red) exhibit antimiR activities as revealed by the decrease in microRNA-21 levels (30%).

transfecting agent) of HeLa cells with (i) a 5 nM suspension of LON-QDs (diC15-antimiR-1 and diC15-antimiR-2 LON/DOPC-QD), which corresponds to a LON concentration of 100 nM, (ii) nontagged QDs, or (iii) 1 μM LONs (diC15antimiR-1 and diC15-antimiR-2) alone for 3 days. Results were compared with those obtained from the transfection via lipofectamine of a scramble sequence, of the antimiR sequence, and of antimiR-LONs (diC15-antimiR-1 and diC15-antimiR-2). Under these conditions, quantitative RT-PCR experiments show that LONs alone (antimiR-1 and antimiR-2) and nontagged QDs (QD) cannot hybridize with microRNA-21 as judged by residual microRNA-21 levels (Figure 9).

In contrast, LONs (antimiR-1 and antimiR-2) and antimiR ON transfected by using lipofectamine hybridized with microRNA-21, demonstrating that the conjugation of a lipid at the oligonucleotide 5′-extremity did not inhibit its *in cellulo* hybridization. Despite the fact that LON structures have been reported to efficiently inhibit hepatitis C virus translation in human hepatic Huh7 cells,[31] unexpectedly, LONs alone (antimiR-1 and antimiR-2) were not efficient against microRNA-21 in HeLa cells. Also, in contrast with nontagged QDs, we found that LON-QDs were exclusively hybridized on microRNA-21 in a manner independent of the conjugation linker (antimiR-1 and antimiR-2). To gain insight into the intracellular behavior of LON-QDs, fluorescence colocalization experiments were performed by anchoring fluorescent LON (FAM) on QDs. After incubation for 24 h, overlapped (yellow) as well as dissociated (green and red) colors appear, revealing partial dissociation of LON from QDs (Figure 10). Nevertheless, in contrast to previous results reporting the requirement of transfecting or targeting agents for siRNA-QDs to induce a biological effect,[36] the LON-QD nanoplatform developed in our study delivered efficient LONs, which can hybridize to its cytoplasm ON target. Altogether, our results emphasize the robustness of this innovative QD platform that combines cell internalization, endosomal escape, and hybridization with the intracellular target ON.

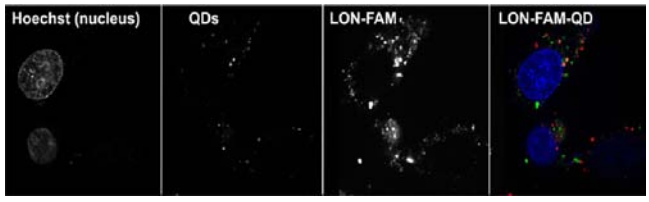

Figure 10. Confocal images of a fluorescent-LON-QD platform after incubation in HeLa cells for 24 h: green for fluorescent LON (FAM-LON), blue for Hoechst 33342 nucleus staining, and red for QD platforms.

CONCLUSION

MicroRNAs are regulators of numerous cellular pathways and are involved in many diseases, including cancers. Hence, members of this class of small nucleic acid are currently emerging as new promising therapeutic targets and/or potentially relevant biomarkers.[38,39] In this context, the LON-QD nanoplatform developed in this study offers new opportunities for future combined diagnosis and therapy applications. Our results demonstrate that LONs featuring molecular recognition principles afford an original and powerful approach to addressing the QD functionalization issue. The described technology uses a single principle based on a nanoparticle imaging core (CdSe/ZnS) surrounded by amphiphilic oligonucleotides. Using different techniques such as fluorescence spectroscopy, transmission electron microscopies, and light scattering (DLS), we identified key physical and structural characteristics that affect the different steps of the nanoplatform implementation. Surface plasmon resonance (SPR) studies were then performed to evaluate the affinity and specificity of the nanoplatform for the targeted microRNA. Results indicate that the kinetics and thermodynamics of duplex formation at the surface of the QDs remain essentially unaffected compared to those of formation of the same duplex free in solution or at the surface of a liposome. These proof-of-principle investigations demonstrate that recognition and detection of RNA such as miRNAs is feasible, thus paving the way for the development of an LON-based QD nanoplatform.

MATERIALS AND METHODS

Synthesis. *General Procedures and Materials.* All the compounds were purchased from Sigma-Aldrich, Fluka, and Alfa Aesar unless otherwise noted. Solvents of the highest

dx.doi.org/10.1021/bc400157z | *Bioconjugate Chem.* 2013, 24, 1345−1355

quality were purchased from Sigma-Aldrich for reactions and from VWR for other uses. All the reactions were conducted under a nitrogen atmosphere unless otherwise stated. Analytical thin layer chromatography (TLC) was performed on precoated silica gel F_{254} plates with a fluorescent indicator from Merck. The detection of compounds was accomplished using a UV light (254 nm) and visualized on TLC plates by subsequent spraying with a 10% concentrated H_2SO_4 solution in ethanol, followed by heating. Column chromatography was performed with flash silica gel (0.04−0.063 mm) from Merck. All the compounds were characterized using ^1H, ^{13}C, and ^{31}P nuclear magnetic resonance (NMR) spectroscopy. These NMR spectra were recorded (in $CDCl_3$ obtained from Eurisotop) on a BRUKER Avance DPX-300 spectrometer (^1H at 300.13 MHz, ^{13}C at 75.46 MHz, and ^{31}P at 121.49 MHz). The chemical shifts (δ) are given in parts per million relative to tetramethylsilane or residual solvent peaks ($CHCl_3$, ^1H 7.26, ^{13}C 77.0). The coupling constants (J) are given in hertz; the peak multiplicity is reported as follows: s for singlet, bs for broad singlet, d for doublet, t for triplet, and m for multiplet. High-resolution electrospray ionization (HR ESI) and matrix-assisted laser desorption ionization time-of-flight (MALDI-TOF) mass spectra were recorded by CESAMO (Bordeaux, France) on a QStar Elite mass spectrometer (Applied Biosystems). The instrument is equipped with an ESI source, and spectra were recorded in negative mode. The electrospray needle was maintained at 4500 V and operated at room temperature. Samples were introduced by injection through a 10 μL sample loop into a 200 μL/min flow of methanol from the LC pump.

2′,3′-O-16-Hentriacontanylidenuridine ***1***. 2′,3′-*O*-16-Hentriacontanylidenuridine was synthesized according to the literature procedure.[32] The data agreed with the literature values.

2′,3′-O-16-Hentriacontanyliden-5′-O-propargyluridine ***2***. Anhydrous THF (10 mL) was added under nitrogen to 2′,3′-*O*-16-hentriacontanylidenuridine **1** (677 mg, 1 mmol). The mixture was cooled at 0 °C, and NaH (36 mg, 1.5 mmol) was added. Propargyl bromide (148.7 mg, 1.25 mmol) was then added at room temperature. The reaction mixture was maintained at 50 °C while being stirred for 24 h. The reaction was stopped by addition of methanol (1 mL). The THF was removed under reduced pressure. The residual solid was dissolved in 25 mL of DCM and was washed successively twice with water (5 mL) and once with brine (10 mL). The organic phase was dried on Na_2SO_4 and evaporated under reduced pressure. Product **2** was isolated after purification on silica gel (ethyl acetate/hexane/TEA mixture from 19/80/1 to 29/70/1). Yield: 445 mg (62.2%). R_f = 0.43 (29/270/1 ethyl acetate/hexane/TEA). ^1H NMR (300 MHz, $CDCl_3$): δ 0.86 (t, 6H, J = 6.9 Hz, $2CH_3$ of chain), 1.24 (s, 52H, $26CH_2$ of chain), 1.52−1.75 [m, 4H, CH_2-C-CH_2 (chain)], 2.46 (t, 1H, J = 2.3 Hz, -C≡CH), 3.69−3.88 (m, 2H, 2H5′), 4.17 (t, 2H, J = 2.7 Hz CH_2-C≡), 4.37−4.40 (s, 1H, H2′), 4.78−4.85 (m, 2H, H4′, H3′), 5.69 [d, 1H, J = 8.1 Hz, H-5 (base)], 5.82 (s, 1H, H1′), 7.48 [d, 1H, J = 8.1 Hz, H-6 (base)], 9.81 [s, 1H, -NH (base)]. ^{13}C NMR (75 MHz, $CDCl_3$): δ 14.1 (CH_3 chain), 22.6 (CH_2-CH_3 chain), 23.4 (CH_2-CH_2-C-), 24.1 (CH_2-CH_2-C-), 29.3−29.8 (CH_2 chain), 31.6 (CH_2-CH_2-CH_3 chain), 36.9 (CH_2-C-CH_2), 58.5 (CH_2-C≡), 69.9 (C5′ sugar), 75.2 (-C≡CH), 78.7 (-C≡CH), 81.1 (C3′ sugar), 85.1 (C4′ sugar), 86.0 (C2′ sugar), 93.7 (C1′ sugar), 102.1 (C5 base), 118.0 (C, ketal), 141.8 (C6 base), 150.1 [C═O(2) base], 163.8 [C═O(4) base]. High-resolution ESI MS [M + Na]$^+$: theoretical m/z 737.5439, observed m/z 737.5454.

5′-Azido-5′-deoxythymidine ***3***. 5′-Azido-5′-deoxythymidine **3** was synthesized according to the literature procedure.[40,31] The data agreed with the literature values.

1-((2R,4S,5R)-5-((5-((((3aR,4R,6R,6aR)-6-(2,4-Dioxo-3,4-dihydropyrimidin-1(2H)-yl)-2,2-dipentadecyltetrahydrofuro-[3,4-d][1,3]dioxol-4-yl)methoxy)methyl)-1H-1,2,3-triazol-1-yl)methyl)-4-hydroxytetrahydrofuran-2-yl)-5-methylpyrimidine-2,4(1H,3H)-dione ***4***. 2′,3′-*O*-16-Hentriacontanyliden-5′-*O*-propargyluridine **2** (445 mg, 0.63 mmol), sodium ascorbate (25 mg, 0.13 mmol), and copper sulfate (10 mg, 0.063 mmol) were added to 5′-azido-5′-deoxythymidine **6** (167 mg, 0.63 mmol) in a water/THF mixture (1/1) (20 mL). The reaction mixture was maintained at 65 °C while being stirred for 10 h. The mixture was cooled to room temperature, and the solvent was evaporated. The residual solid was dissolved in DCM (100 mL) and washed successively twice with water (20 mL) and once with brine (20 mL). The organic phase was dried on Na_2SO_4 and evaporated under reduced pressure. Product **4** was isolated after purification on silica gel (6/93/1 MeOH/ethyl acetate/TEA). Yield: 480 mg (78.5%). R_f = 0.32 (6/93/1 MeOH/ethyl acetate/TEA). ^1H NMR (300 MHz, $CDCl_3$): δ 0.87 (t, 6H, J = 6.5 Hz, $2CH_3$ of chain), 1.25 (s, 52H, $26CH_2$ of chain), 1.48−1.78 [m, 4H, CH_2-C-CH_2 (chain)], 1.86 (s, 3H, CH_3 thymine base), 2.31−2.54 [m, 2H, H2″ (sugar of thymidine)], 3.68−3.82 [m, 2H, H5′ (sugar of uridine)], 4.18−4.85 (m, 10H, -O-CH_2, H2′, H3′, H4′, H3″, H4″, H5″, -OH), 5.55 [d, 1H, J = 8.1 Hz, H-5 (uracil base)], 5.77 [s, 1H, H1′ (sugar of uridine)], 6.06 [t, 1H, J = 6.4 Hz, H1″ (sugar of thymidine)], 6.97 (s, 1H, triazole), 7.47 [d, 2H, J = 8.1 Hz, H-6 (uracil base)], 7.70 [s, 1H, H-6 (thymine base)], 9.79 [s, 1H, -NH (uracil base)], 10.08 [s, 1H, -NH (thymine base)]. ^{13}C NMR (75 MHz, $CDCl_3$): δ 12.3 (CH_3 base), 14.0 (CH_3 chain), 22.6 (CH_2-CH_3 chain), 23.4 (CH_2-CH_2-C-), 24.1 (CH_2-CH_2-C-), 29.3−29.6 (CH_2 chain), 31.8 (CH_2-CH_2-CH_3 chain), 36.9 (CH_2-C-CH_2), 38.4 (C2″), 51.5 (C5″), 64.3 (-O-CH_2), 70.4 (C3″), 71.4 (C5′), 81.0 (C4″), 84.1 (C3′), 85.1 (C4′), 86.3 (C2′), 86.8 (C1″), 93.9 (C1′), 101.4 (C5 thymine base), 111.1 (C5 uracil base), 117.7 (C, ketal), 124.5 (-CH triazole), 137.2 (C6 thymine base), 142.3 (C6 uracil base), 143.8 (═C-triazole), 150.2 [C═O(2) uracil base], 150.8 [C═O(2) thymine base], 164.3 [C═O(4) thymine base], 164.6 [C═O(4) uracil base]. High-resolution ESI MS [M + H]$^+$: theoretical m/z 982.6587, observed m/z 982.6613.

2-Cyanoethyl (2R,3S,5R)-2-((5-((((3aR,4R,6R,6aR)-6-(2,4-Dioxo-3,4-dihydropyrimidin-1(2H)-yl)-2,2-dipentadecyltetrahydrofuro[3,4-d][1,3]dioxol-4-yl)methoxy)-methyl)-1H-1,2,3-triazol-1-yl)methyl)-5-(5-methyl-2,4-dioxo-3,4-dihydropyrimidin-1(2H)-yl)tetrahydrofuran-3-yl Diisopropylphosphoramidite ***5***. Under argon, freshly distilled DIPEA (127 mg, 0.98 mmol) and 2-cyanoethyl-*N*,*N*-diisopropylchlorophosphoramidite (174 mg, 0.74 mmol) were added to nucleolipid **4** (480 mg, 0.49 mmol) in dry DCM (10 mL). The reaction mixture was maintained at room temperature while being stirred for 6 h. DCM (5 mL) was added, and the mixture was washed successively twice with $NaHCO_3$ (5% in water, 5 mL) and once with brine (5 mL). The organic phase was dried on Na_2SO_4 and evaporated under reduced pressure. Product **5** was isolated after purification on silica gel (69/30/1 ethyl acetate/hexane/TEA). Yield: 313 mg (54.4%). R_f = 0.28 (59/40/1 ethyl acetate/hexane/TEA). ^1H NMR (300 MHz, $CDCl_3$): δ 0.85 (t, 6H, J = 6.4 Hz, $2CH_3$ of chain), 1.17−1.19

(d, J = 6.6 Hz, 12H, 4CH_3 of isopropyl group), 1.22 (s, 52H, 26CH_2 of chain), 1.46−1.77 [m, 4H, CH_2-C-CH_2 (chain)], 1.85 (s, 3H, CH_3 thymine base), 2.33−2.80 [m, 6H, 2H of two isopropyl group, 2H of CH_2-CN, 2H2″ (sugar of thymidine)], 3.39−3.68 [m, 4H, 2H-OCH_2CH_2CN, 2H5′ (sugar of uridine)], 4.19−4.87 (m, 9H, -O-CH_2, H2′, H3′, H4′, H3″, H4″, H5″), 5.61 [d, 1H, J = 8.1 Hz, H-5 (uracil base)], 5.85 [s, 1H, H1′ (sugar of uridine)], 6.00−6.11 [m, 1H, H1″ (sugar of thymidine)], 6.94 (s, 1H, triazole), 7.49 [d, 2H, J = 8.1 Hz, H-6 (uracil base)], 7.68 [s, 1H, H-6 (thymine base)]. ^{31}P NMR (121.49 MHz, $CDCl_3$): δ 152.3 (d, P). High-resolution ESI MS $[M + Na]^+$: theoretical m/z 1204.7485, observed m/z 1204.7516.

LON Synthesis. Model, antimiR, complementary sequences and scramble oligonucleotides as well as LONs were synthesized using a phosphoramidite methodology on an automated Expedite 8909 DNA synthesizer on a micromole scale on a 500 Å primer support (loading of 60−100 μmol/g, Link technologies, Synbase Control Pore Glass) according to the procedure previously described.[29] Yields were good (falling in the range of 15−25%). MALDI-TOF mass analyses were conducted, and values are listed in Table 2.

Table 2

LON	$[M - H]^+$ calcd	$[M - H]^+$ found
C18-model-1	4862	4865
Chol-model-1	5038	5040
diC15-model-2	5456	5050
C18-antimiR-1	7512	7513
diC15-antimiR-1	7921	7922
Chol-antimiR-1	7629	7630
diC15-antimiR-2	7647	7648

Nanoplatform Implementation. *Water Solubilization of QDs by Encapsulation with Phospholipids.* QD CdSe/Zn Score-shell (10 mg/mL in toluene) was purchased from Evidentech. Ten microliters (0.25 nmol) of this solution was added to a flask, mixed with 1 mL of chloroform, and dried under vacuum for 2 h. QDs were then suspended in 5 mL of chloroform with 2.50 μmol of lipids or nucleolipids. Different molecules were used: DOPC (1,2-dioleoyl-*sn*-glycero-3-phosphocholine from bachem), PUPC (palmitic uridine phosphocholine), and a PUOH (palmitic uridine)/PUPC (75/25) mixture. The resulting mixture was stirred and distributed in several tubes to improve the formation of films after drying. Chloroform evaporation was performed using a rotary evaporator at 30 °C and 100 rpm under reduced pressure. After complete evaporation of the chloroform, the tubes were heated at 80 °C for 1 min. Then a total of 5 mL of Milli-Q Water was added to the tubes, and the solution was vigorously stirred to yield QD solubilization. QD micelles were isolated from QD aggregates by centrifugation at 14000 rpm for 10 min. Additional phospholipids were removed by ultracentrifugation at 300000g for 25 min in a 20% sucrose solution. The supernatant was discarded, and the QD micelles were resuspended in water. Sucrose was eliminated by centrifugation using a Sartorius Vivaspin 500 disposable system (cutoff of 10 kDa). The QD micelles were then stored in water at 4 °C in the dark.

QD Functionalization by LONs. For the preparation of functionalized QDs, we used LONs, the hydrophobic chains of which interact with the lipidic coating at the QD surface.

Solubilized QDs were prepared at 1 μg/mL in an aqueous buffer [50 mM Na_2HPO_4 and 150 mM NaCl (pH 7)]. One milliliter of this suspension (2.5 pmol) was vortexed with 10 μL of a 12.5 μM LON solution and incubated at 37 °C for 1 h. Excess free LON was removed by centrifugation using Millipore filters (cutoff of 30 kDa) and quantified by absorbance measurement using a nanodrop UV−vis spectrophotometer. The difference between the starting material and unbound LONs allows the determination of the number of LONs per QD.

Physicochemical Characterization. *Fluorescence Spectroscopy.* Fluorescence spectra of organic, solubilized, and functionalized QDs were measured in a small-volume quartz cuvette and acquired using an LS 55 Perkin-Elmer instrument (xenon source excitation, FL WinLab software). Samples were excited at 350 nm (15 nm slit), and emission profiles were recorded from 555 to 655 nm (5 nm slit).

TEM Experiments. TEM studies were performed on a HITACHI H7650 electron microscope in high-resolution mode, at the BIC platform (Bordeaux Imaging Center). The software used for image acquisition was Digital Micrograph (Gatan). Ten microliters of the QD sample was transferred onto a carbon Formvar-coated 200 mesh nickel grid and dried for 10 min before being observed.

DLS. The particle size and ζ potential were mesured on a Zetasizer Nano-ZS instrument (Malvern Instrument). All measurements were taken at 25 °C with 100 μL of a QD suspension diluted into 1 mL of Milli-Q Water. The samples were illuminated at 633 nm with a He/Ne laser, and the scattered light was detected at an angle of 175°. The scattering data were analyzed via a non-negative least-squares algorithm (GP) as implemented in the Zetasizer Nano software.

***In Vitro* Hybridization Studies.** *Surface Plasmon Resonance (SPR).* SPR experiments were performed on a Biacore TM 3000 apparatus (Biacore, GE Healthcare, Uppsala, Sweden) with an L1 sensor chip for direct entrapment of lipid membrane vesicles. L1 sensor chips were prepared by injecting a 1 min pulse of 40 mM *N*-octyl β-glucopyranoside (Sigma) followed by two 1 min pulses of a 50/50 (v/v) mixture of 100 mM HCl and 2-propanol, at a rate of 100 μL/min in water.

Nontagged QDs and LON-QDs were diluted to 1 μg/mL in running buffer [50 mM NaH_2PO_4 and 150 mM NaCl (pH 7) at 20 °C] and captured (3500−4000 RU) across isolated flow cells at a rate of 5 μL/min by injection of ∼50 μL of QD suspensions. Approximately ten 1 min pulses of a freshly prepared 10 mM NaOH solution were injected to eliminate nonspecific immobilization.

Experiments, performed in at least triplicate, were conducted at 25 °C in running buffer. Different ONs (fully or partially complementary and scramble sequences) were injected into the running buffer at a rate of 20 μL/min across the sensor surface (QD and QD-free surfaces) in a single step. Regeneration was achieved with two 1 min pulses of a 10 mM NaOH solution followed by a 1 min pulse of running buffer. Three concentrations of ON were injected to determine the kinetic parameters.

All data were double-referenced to remove instrument noise and contributions of the buffer to the signal. The association and dissociation rate constants (k_{on} and k_{off}, respectively) were determined from direct curve fitting of the sensorgrams using BiaEval version 4.1 (Biacore), assuming a simple reversible mechanism according to eqs 1 and 2, for the association and dissociation phases, respectively:

$$dRU/dt = k_{on}[ligand]RU_{max} - (k_{on}[ligand] + k_{off})RU \quad (1)$$

$$dRU/dt = -k_{off}RUt_0e^{-(k-1)}(t - t_0) \quad (2)$$

where RU is the signal response, RU_{max} the maximal response level, RUt_0 the response at the beginning of the dissociation phase, and [ligand] the molar concentration of the injected ONs. The binding equilibrium constant, k_d, was calculated as k_{off}/k_{on}.

Intracellular Hybridization Studies. *Cell Culture.* HeLa cells obtained from C. Steadel (Inserm U869, Bordeaux, France) were cultured in DMEM containing 10% fetal bovine serum (FBS) at 37 °C in a humidified 5% CO_2 atmosphere.

Cell Uptake. HeLa cells were seeded in culture Well removable chambered coverglass for cell culture at a density of 5×10^4 cells/well in DMEM containing 10% FBS and cultured overnight. After incubation for 4 h with 2.5 nM nontagged QDs and LON-QDs, excess unbound QDs were removed when the samples were washed three times with phosphate-buffered saline (PBS, pH 7.4). All samples were incubated with 1 μg/mL Hoechst 33342 (to label DNA so nucleus) and 50 μg/mL Concanavalin A AlexaFluor 488 (to label cell membrane). All the fluorescent markers were purchased from Molecular Probes. Then the cells were washed twice with PBS and mounted in SlowFade Gold mounting medium (Invitrogen). The slides were observed by epifluorescence using a Zeiss Axiovert fluorescence microscope (40× immersion objective) or confocal laser scanning microscope (CLSM, Zeiss Axiovert 200M microscope) coupled with a Zeiss LSM 510 scanning device. The inverted microscope was equipped with a Plan-Apochromat 63× objective (NA = 1.4) and with a temperature-controlled stage. Images were collected using the different excitation (ex) lines and emission (em) filters: QDs, 350 nm (ex) and 620 nm (em); Concanavalin A AlexaFluor 488, 495 nm (ex) and 519 nm (em); Hoechst 33342, 350 nm (ex) and 461 nm (em). Phase-contrast images were collected using 633 nm laser illumination. Composite merged images were produced using the LSM Image Browser (Zeiss).

Colocalization Studies. HeLa cells were seeded in culture Well removable chambered coverglass for cell culture at a density of 5×10^4 cells/well in DMEM containing 10% FBS and cultured overnight. After incubation for 24 h with 2.5 nM FAM-LON-QD, excess unbound QDs were removed when the samples were washed three times with phosphate-buffered saline (PBS, pH 7.4). All samples were incubated with 1 μg/mL Hoechst 33342 (to label DNA so nucleus). Then the cells were washed twice with PBS and mounted in SlowFade Gold mounting medium (Invitrogen). The slides were observed via a confocal laser scanning microscope (Zeiss Axiovert 200M microscope) coupled with a Zeiss LSM 510 scanning device. The inverted microscope was equipped with a Plan-Apochromat 63× objective (NA = 1.4) and with a temperature-controlled stage. Images were collected using the different excitation (ex) lines and emission (em) filters: QDs, 350 nm (ex) and 620 nm (em); Fluorescein FAM, 492 nm (ex) and 517 nm (em); Hoechst 33342, 350 nm (ex) and 461 nm (em). Phase-contrast images were collected using 633 nm laser illumination. Composite merged images were produced using the LSM Image Browser (Zeiss).

Quantitative RT-PCR. Twenty-four hours before being transfected or incubated, HeLa cells were seeded at a density of 5×10^4 cells/well in a 24-well plate in DMEM containing 10% FBS. HeLa cells were then transfected with 100 nM antimiR-ON or antimiR-LON (diC15-antimiR-1 and diC15-antimiR-2) using the lipofectamine as the transfecting agent according to the manufacturer's instructions or with 5 nM nontagged QDs and antimiR-LON-QDs (which correspond to 100 nM antimiR-LON) or with 1 μM antimiR-LONs (diC15-antimiR-1 and diC15-antimiR-2). After being incubated for 72 h, cells were washed three times with phosphate-buffered saline (PBS, pH 7.4) to remove excess unbound QDs, and total RNA was extracted using Trizol reagent (Invitrogen), according to the manufacturer's protocol. RNA concentrations were determined by a NanoDrop spectrophotometer. Expression of mature miR-21 was assessed by miR quantitative RT-PCR using microRNA specific looped RT primers and TaqMan probes as recommended by the manufacturer (Applied Biosystems). Reverse transcription occurred for 30 min at 16 °C and then for 30 min at 42 °C and was stopped at 85 °C for 5 min. The cDNAs thus obtained were used for real-time quantitative PCR performed in triplicate in the Qiagen Rotor-Gene Q apparatus using the following program: 10 min at 95 °C to activate the Taq polymerase and then 40 cycles (15 s at 95 °C and 60 s at 60 °C). U6snRNA was used as an internal control, and relative levels of expression were calculated using the comparative Ct method. PCR was performed in triplicate using the 7300 Real-Time PCR system (Applied Biosystems).

■ ASSOCIATED CONTENT

Ⓢ Supporting Information

NMR, mass spectra, and HPLC profiles. This material is available free of charge via the Internet at http://pubs.acs.org.

■ AUTHOR INFORMATION

Corresponding Author

*E-mail: isabelle.bestel@inserm.fr (I.B.) and philippe.barthelemy@inserm.fr (P.B.).

Author Contributions

I.B. and P.B. contributed equally to this work.

Notes

The authors declare no competing financial interest.

■ ACKNOWLEDGMENTS

We acknowledge financial support from the French National Agency (ANR) in the frame of its program in Nanosciences and Nanotechnologies (NANAN Project ANR-08-NANO-028). We thank the SERCOMI Centre and the BIC platform for technical assistance during TEM and fluorescence observations, respectively. Many thanks to Cathy Staedel for her advice during the biological evaluation. P.B. acknowledges financial support from the Army Research Office.

■ REFERENCES

(1) Sanderson, K. (2009) Quantum dots go large. *Nature 459*, 760–761.

(2) Hildebrandt, N. (2011) Biofunctional quantum dots: Controlled conjugation for multiplexed biosensors. *ACS Nano 5*, 5286–5290.

(3) Mattoussi, H., Palui, G., and Na, H. B. (2012) Luminescent quantum dots as platforms for probing in vitro and in vivo biological processes. *Adv. Drug Delivery Rev. 64*, 138–166.

(4) Gao, X., Yang, L., Petros, J. A., Marshall, F. F., Simons, J. W., and Nie, S. (2005) In vivo molecular and cellular imaging with quantum dots. *Curr. Opin. Biotechnol. 16*, 63–72.

(5) Pinaud, F., Michalet, X., Bentolila, L. A., Tsay, J. M., Doose, S., Li, J. J., Iyer, G., and Weiss, S. (2006) Advances in fluorescence imaging with quantum dot bio-probes. *Biomaterials 27*, 1679–1687.

(6) Dahan, M., Lévi, S., Luccardini, C., Rostaing, P., Riveau, B., and Triller, A. (2003) Diffusion dynamics of glycine receptors revealed by single-quantum dot tracking. *Science 302*, 442−445.
(7) Michalet, X., Pinaud, F. F., Bentolila, L. A., Tsay, J. M., Doose, S., Li, J. J., Sundaresan, G., Wu, A. M., Gambhir, S. S., and Weiss, S. (2005) Quantum dots for live cells, in vivo imaging, and diagnostics. *Science 307*, 538−544.
(8) Gill, R., Zayats, M., and Willner, I. (2008) Semiconductor Quantum Dots for Bioanalysis. *Angew. Chem., Int. Ed. 47*, 7602−7625.
(9) Yaghini, E., Seifalian, A. M., and MacRobert, A. J. (2009) Quantum dots and their potential biomedical applications in photosensitization for photodynamic therapy. *Nanomedicine 4*, 353−363.
(10) Sablon, K. A. (2009) Towards Quantum Computing: A Hybrid Approach That Will Unleash a Plethora of New QD Nanostructures, Bringing Us a Step Further to Laterally Coupled QDs. *Nanoscale Res. Lett. 4*, 1254−1255.
(11) Hyeon-Deuk, K., and Prezhdo, O. V. (2012) Photoexcited electron and hole dynamics in semiconductor quantum dots: Phonon-induced relaxation, dephasing, multiple exciton generation and recombination. *J. Phys.: Condens. Matter 24*, 63201.
(12) Panzer, M. J., Aidala, K. E., and Bulović, V. (2012) Contact printing of colloidal nanocrystal thin films for hybrid organic/quantum dot optoelectronic devices. *Nano Rev. 3*, 16144−16151.
(13) Xu, P. F., Ji, H. M., Yang, T., Xu, B., Ma, W. Q., and Wang, Z. (2011) The research progress of quantum dot lasers and photodetectors in China. *J. Nanosci. Nanotechnol. 11*, 9345−9356.
(14) Vannoy, C. H., Tavares, A. J., Noor, M. O., Uddayasankar, U., and Krull, U. J. (2011) Biosensing with quantum dots: A microfluidic approach. *Sensors 11*, 9732−9763.
(15) Boeneman, K., Deschamps, J. R., Buckhout-White, S., Prasuhn, D. E., Blanco-Canosa, J. B., Dawson, P. E., Stewart, M. H., Susumu, K., Goldman, E. R., Ancona, M., and Medintz, I. L. (2010) Quantum Dot DNA Bioconjugates: Attachment Chemistry Strongly Influences the Resulting Composite Architecture. *ACS Nano 4*, 7253−7266.
(16) Dubertret, B., Skourides, P., Norris, D. J., Noireaux, V., Brivanlou, A. H., and Libchaber, A. (2002) In Vivo Imaging of Quantum Dots Encapsulated in Phospholipid Micelles. *Science 298*, 1759−1762.
(17) Lees, E. E., Nguyen, T.-L., Clayton, A. H. A., and Mulvaney, P. (2009) The preparation of colloidally stable, water-soluble, biocompatible, semiconductor nanocrystals with a small hydrodynamic diameter. *ACS Nano 3*, 1121−1128.
(18) Mitchell, G. P., Mirkin, C. A., and Letsinger, R. L. (1999) Programmed Assembly of DNA Functionalized Quantum Dots. *J. Am. Chem. Soc. 121*, 8122−8123.
(19) Medintz, I. L., Berti, L., Pons, T., Griner, A. F., English, S. H., Alessandrini, A., Pacci, P., and Mattoussi, H. (2007) A reactive peptide linker for self-assembling hybrid quantum dot-DNA bioconjugates. *Nano Lett. 7*, 1741−1748.
(20) Diamandis, E. P., and Christopoulos, T. K. (1991) The Biotin (Strept)Avidin System: Principles and Applications in Biotechnology. *Clin. Chem. 37*, 625−636.
(21) Lidke, D. S., Nagy, P., Jovin, T. M., and Arndt-Jovin, D. J. (2007) Biotin-ligand complexes with streptavidin quantum dots for in vivo cell labeling of membrane receptors. *Methods Mol. Biol. 374*, 69−79.
(22) Medintz, I., Uyeda, H., Goldman, E., and Mattoussi, H. (2005) Quantum dot bioconjugates for imaging, labelling and sensing. *Nat. Mater. 4*, 435−446.
(23) Lee, J., Choi, Y., Kim, J., Park, E., and Song, R. (2009) Positively charged compact quantum dot-DNA complexes for detection of nucleic acids. *ChemPhysChem 10*, 806−811.
(24) Algar, W. R., and Krull, U. J. (2011) Characterization of the adsorption of oligonucleotides on mercapto propionic acid coated CdSe/ZnS quantum dots using fluorescence energy transfer. *J. Colloid Interface Sci. 359*, 148−154.
(25) Patwa, A., Gissot, A., Bestel, I., and Barthélémy, P. (2011) Hybrid lipid oligonucleotide conjugates: Synthesis, self-assemblies and biomedical applications. *Chem. Soc. Rev. 40*, 5844−5854.
(26) Gosse, C., Boutorine, A., Aujard, I., Chami, M., Kononov, A., Cogné-Laage, E., Allemand, J.-F., Li, J., and Jullien, L. (2004) Micelles of lipid-oligonucleotide conjugates: Implications for membrane anchoring and base pairing. *J. Phys. Chem. B 108*, 6485−6497.
(27) Banchelli, M., Baldelli Bombelli, F., Berti, D., and Baglioni, P. (2009) Soft hybrid nanostructures composed of phospholipid liposomes decorated with oligonucleotides. *Methods Enzymol. 464*, 249−277.
(28) Banchelli, M., Gambinossi, F., Durand, A., Caminati, G., Broxn, T., Berti, D., and Baglioni, P. (2010) Modulation of density and orientation of amphiphilic DNA on phospholipid membranes. II. Vesicles. *J. Phys. Chem. B 114*, 7438−7358.
(29) Gissot, A., Di Primo, C., Bestel, I., Giannone, G., Chapuis, H., and Barthélémy, P. (2008) Sensitive liposomes encoded with oligonucleotide amphiphiles: A biocompatible switch. *Chem. Commun. 43*, 5550−5552.
(30) Pan, X., Wang, Z. X., and Wang, R. (2011) MicroRNA-21: A novel therapeutic target in human cancer. *Cancer Biol. Ther. 10*, 1224−1232.
(31) Godeau, G., Staedel, C., and Barthélémy, P. (2008) Lipid-conjugated oligonucleotides via "click chemistry" efficiently inhibit hepatitis C virus translation. *J. Med. Chem. 51*, 4374−4376.
(32) Moreau, L., Camplo, M., Wathier, M., Taib, N., Laguerre, M., Bestel, I., Grinstaff, M. W., and Barthélémy, P. (2008) Real time imaging of supramolecular assembly formation via programmed nucleolipid recognition. *J. Am. Chem. Soc. 130*, 14454−14455.
(33) Taib, N., Aimé, A., Moreau, L., Camplo, M., Houmadi, S., Desbat, B., Laguerre, M., Grinstaff, M., Bestel, I., and Barthélémy, P. (2012) Formation of supramolecular systems via directed nucleoside-lipide recognition. *J. Colloid Interface Sci. 377*, 122−130.
(34) Taib, N., Aimé, A., Houmadi, S., Castano, S., Barthélémy, P., Laguerre, M., and Bestel, I. (2012) Interactions of nucleolipids with oligonucleotides: Molecular modelling and physicochemical studies. *Langmuir 28*, 7452−7460.
(35) Carion, O., Mahler, B., Pons, T., and Dubertret, B. (2007) Synthesis, encapsulation, purification and coupling of single quantum dots in phospholipid micelles for their use in cellular and in vivo imaging. *Nat. Protoc. 2*, 2383−2390.
(36) Xiao, Y., Forry, S. P., Gao, X., Holbrook, R. D., Telford, W. G., and Tona, A. (2010) Dynamics and mechanisms of quantum dot nanoparticle cellular uptake. *J. Nanobiotechnol. 8*, 13−21.
(37) Derfus, A. M., Chen, A. A., Min, D.-H., Ruoslahti, E., and Bhatia, S. N. (2007) Targeted quantum dot conjugates for siRNA delivery. *Bioconjugate Chem. 18*, 1391−1396.
(38) Kim, E., Yang, J., Park, J., Kim, S., Kim, N. H., Yook, J. I., Suh, J.-S., Haam, S., and Huh, Y.-M. (2012) Consecutive Targetable Smart Nanoprobe for Molecular Recognition of Cytoplasmic microRNA in Metastatic Breast Cancer. *ACS Nano 6*, 8525−8535.
(39) Dorvel, B. R., Reddy, B., Go, J., Duarte Guevara, C., Salm, E., Alam, A. M., and Bashir, R. (2012) Silicon Nanowires with High-k Hafnium Oxide Dielectrics for Sensitive Detection of Small Nucleic Acid Oligomers. *ACS Nano 6*, 6150−6164.
(40) Hiebl, J., Zbiral, E., Balzarini, J., and De Clercq, E. (1991) Synthesis and antiretrovirus properties of 5′-isocyano-5′-deoxythymidine, 5′-isocyano-2′,5′-dideoxyuridine, 3′-azido-5′-isocyano-3′,5′-dideoxythymidine, and 3′-azido-5′-isocyano-2′,3′,5′-trideoxyuridine. *J. Med. Chem. 34*, 1426−1430.